Anyonic self-induced disorder in a stabilizer code: Quasi many-body localization in a translational invariant model

H. Yarloo,[1] A. Langari,[1,2,*] and A. Vaezi[3]

[1]*Department of Physics, Sharif University of Technology, P.O.Box 11155-9161, Tehran, Iran*

[2]*Center of excellence in Complex Systems and Condensed Matter (CSCM), Sharif University of Technology, Tehran 14588-89694, Iran*

[3]*Department of Physics, Stanford University, Stanford, California 94305, USA*

(Received 20 March 2017; revised manuscript received 28 December 2017; published 7 February 2018)

We enquire into the quasi many-body localization in topologically ordered states of matter, revolving around the case of Kitaev toric code on the ladder geometry, where different types of anyonic defects carry different masses induced by environmental errors. Our study verifies that the presence of anyons generates a complex energy landscape solely through braiding statistics, which suffices to suppress the diffusion of defects in such clean, multicomponent anyonic liquid. This nonergodic dynamics suggests a promising scenario for investigation of quasi many-body localization. Computing standard diagnostics evidences that a typical initial inhomogeneity of anyons gives birth to a glassy dynamics with an exponentially diverging time scale of the full relaxation. Our results unveil how self-generated disorder ameliorates the vulnerability of topological order away from equilibrium. This setting provides a new platform which paves the way toward impeding logical errors by self-localization of anyons in a generic, high energy state, originated exclusively in their exotic statistics.

DOI: 10.1103/PhysRevB.97.054304

I. INTRODUCTION

Many-body localization (MBL) [1–6] generalizes the concept of single particle localization [7] to isolated interacting systems, where many-body eigenstates in the presence of sufficiently strong disorder can be localized in a region of Hilbert space even at nonzero temperature. An MBL system comes along with universal characteristic properties such as area-law entanglement of highly excited states (HES) [5,8], power-law decay and revival of local observables [9,10], logarithmic growth of entanglement [11–14], as well as the violation of "eigenstates thermalization hypothesis" (ETH) [15–17]. The latter raises the appealing prospect of protecting quantum order as well as storing and manipulating coherent information in out-of-equilibrium many-body states [18–22].

Recently it has been questioned [23–32] whether quench disorder is essential to trigger ergodicity breaking or one might observe glassy dynamics in translationally invariant systems, too. In such models initial random arrangement of particles effectively fosters strong tendency toward self-localization characterized by MBL-like entanglement dynamics, exponentially slow relaxation of a typical initial inhomogeneity, and arrival of inevitable thermalization. This asymptotic MBL—tagged quasi MBL [30]—in contrast to the genuine ones, is not necessarily accompanied by the emergence of an infinite number of conserved quantities [33–36].

Here we present a mechanism toward quasi MBL in a family of *clean* self-correcting memories, in particular the Kitaev toric code [37,38] on ladder geometry, a.k.a. the Kitaev ladder (KL) [39,40]. The elementary excitations of KL are associated with pointlike quasiparticles, known as electric (e) and magnetic (m) charges. Our main interest has its roots in the role of nontrivial statistics between anyons that naturally live in (highly) excited states of such models.

Stable topological memories, by definition, need to preserve the coherence of encoded quantum state for macroscopic timescales. However, due to their thermal fragility [41–45], specially far-from-equilibrium [46,47], the problem of identifying a stable low-dimensional quantum memory is still unsecure. One of the major obstacles to this end is that they do not withstand dynamic effects of perturbations whenever a nonzero density of anyons is initially present in the system. Indeed, propagation of even one pair of deconfined anyons around noncontractible loops of the system leads to logical error [47]. In addition, system's dynamics under generic perturbations could be so tangled that the quantum memory equilibrates in the thermal Gibbs state, in which no topological order survives [45].

So far, extensive searches have been carried out to combat the mentioned shortcomings, such as: considering clean cubic [48,49] or higher dimensional codes [50,51] with a more complex structure than the toric one, 2D codes consisting of N-level spins [52] as well as coupling 2D codes to a massless scalar field [53–55]. In particular, exerting an external disorder on a stabilizer code strengthens the stability of topological phase [56] and ensures the single particle localization of Abelian anyons as long as their initial density is below a critical value [57,58]. This disorder-induced glassiness that exponentially suppresses the motion of deconfined anyons (and thus impedes logical errors) makes a topological quantum memory fault tolerant, provided that the perturbed system remains noninteracting. An outstanding question is whether one can exponentially suppress dynamic effects of *generic* local

*langari@sharif.edu

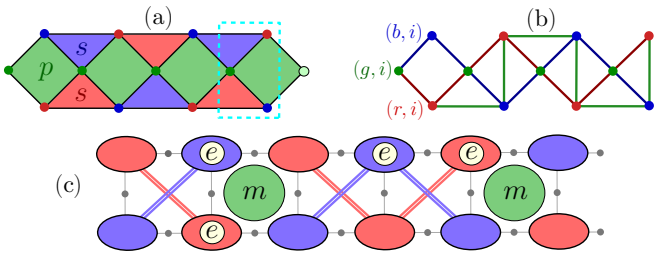

FIG. 1. (a) KL with periodic-boundary condition in leg and open-boundary condition along rungs. Spin-1/2 particles are placed on the $3L$ nodes of the lattice. (b) Multiplying Z operators along the red (blue) line yields dual spin $\mu^x_{r/b,i}$, and a similar string of X operators along the green line defines $\mu^x_{g,i}$. (c) The pictorial demonstration of the dual KL, Eq. (4), for $t_m = 0$.

perturbations in the presence of *arbitrary* (increasing) density of preparatory anyons while preserving essential properties of a feasible quantum memory, i.e., being low dimensional as well as translationally invariant [43].

We supply clear-cut evidences that random configurations of anyons in HES of KL prompts a self-generated disorder purely due to the mutual braiding statistics. Performing a dual mapping suggests that nonzero density of the magnetic charges, as barriers, poses a kinetic constraint on dynamics of the electric ones and hinders the propagation of the *confined* charges on nontrivial class of loops around the cylindrical surface of KL. Subsequently, it is more favorable for the initial information to be encoded in subspaces with a higher density of anyons. Finally, we provide numerical evidences that the effective disorder leads to the existence of an exponentially diverging time scale for dynamical persistence of the initial inhomogeneity, along with an intermediate slow growth of the entanglement entropy, all of which are essential qualities of quasi MBL.

The paper is organized as follows. In Sec. II, we introduce the KL Hamiltonian as the simplest stabilizer code with anyonic excitations. Then, we investigate—how due to mutual exotic statistics—the presence of one kind of anyonic quasiparticles leads to an emergent kinetic constraint which suppresses the dynamics of the other kind. In Sec. III, we uncover anyonic self-localization as a dynamical property of Abelian anyons and classify the observed glassiness as the quasi MBL mechanism. The effect of such dynamical glassiness on the robustness of initial topologically encoded information is presented in Sec. IV. Finally, we summarize our work with discussions in Sec. V and generalize the concept of anyonic self-induced disorder to 2D quantum double models.

II. KITAEV LADDER HAMILTONIAN

KL is composed of L unit cells, each with three sites, that we will refer to as red, green, and blue sites [see Fig. 1(a)], and spin-1/2 particles are placed on the $N = 3L$ nodes of the lattice. The unperturbed Hamiltonian is defined by L plaquette stabilizer, B_p, and $2L$ vertex stabilizer terms on the triangles of the ladder, $A^{r/b}_s$, as follows:

$$\begin{aligned} H^{\mathrm{KL}}_0 &= -j_m \sum_i B_p(i) - j_e \sum_i \left(A^r_s(i) + A^b_s(i)\right), \\ B_p(i) &= Z_{g,i} Z_{r,i} Z_{b,i} Z_{g,i+1}, \\ A^{r/b}_s(i) &= X_{r/b,i-1} X_{g,i} X_{b/r,i}, \end{aligned} \tag{1}$$

where X_i and Z_i are the x and z component of Pauli operators, respectively. We set j_e, $j_m > 0$ and choose an overall energy scale by setting $j_e = 1$. KL can be viewed as the Kitaev toric code with surface termination along the rungs direction (a.k.a. surface code [37]) whose width is one. This model represents $\mathbb{Z}_2 \times \mathbb{Z}_2$ symmetry-protected topological (SPT) order [40] associated to anyonic parities,

$$\mathcal{P}_m = \prod_{i=1}^{L} B_p(i), \quad \mathcal{P}_e = \prod_{s\in r/b} A^{r/b}_s(i), \tag{2}$$

where $\mathcal{P}_m$ and $\mathcal{P}_e$ are magnetic and charge parity operators in the red or blue vertices, respectively (see Appendix. A).

Now we would like to perturb the KL Hamiltonian such that e (charge) and m (flux), corresponding to $A_s = -1$ and $B_p = -1$, respectively, hop across the ladder and gain kinetic energy. To this end we consider the perturbed KL with the generic Ising terms:

$$H^{\mathrm{KL}} = H^{\mathrm{KL}}_0 - t_e \sum_{\langle i,j\rangle \in \partial p} Z_i Z_j - t_m \sum_{i\in \mathrm{legs}} X_i X_{i+1}, \tag{3}$$

where t_e (t_m) is the hopping strength of e (m). Via applying $Z_{g,i} Z_{r,i}$, which commutes with every plaquette and star operator except $A^r_s(i)$ and $A^r_s(i+1)$, an e charge on site (r,i) transfers to $(r,i+1)$. We could also use $Z_{b,i} Z_{g,i+1}$ to carry out the same task. However, $Z_{b,i} Z_{g,i+1} = B_p(i) Z_{g,i} Z_{r,i}$, and therefore the total contribution to the Hamiltonian is $(1 + B_p(i)) Z_{g,i} Z_{r,i}$. That being so, the Ising interactions are coupled to the dynamical $\mathbb{Z}_2$ *gauge field* and the hopping of an e charge from (r,i) to $(r,i+1)$ depends on the value of $B_p(i) = (-1)^{n^m_i}$, which takes into account the parity of m anyon on site (g,i), or equivalently, the mutual braiding statistics of e and m. Hence, the hopping of e is blocked if there is a flux on its way. Likewise, $X_{r,i} X_{b,i+1}$ transports one unit of m charge from plaquette (g,i) to $(g,i+1)$ and vice versa. We could also consider $X_{b,i} X_{r,i+1}$ to reach the same goal. However, $X_{b,i} X_{r,i+1} = A^r_s(i+1) A^b_s(i+1) X_{r,i} X_{b,i+1}$, and again the movement of m is intertwined with the density of e's along its way.

According to the single particle simulations of disordered stabilizer codes [57,58], the motion of anyons is not dramatically affected by exotic braiding phases between anyons of opposite types. On the contrary, in the many-body picture, the transport properties of Abelian anyons might strongly be affected by their exotic statistics, so that e and m as two distinct quasiparticles are able to mutually suppress their own dynamics, even in a clean system. The latter property is the characteristic feature of Falicov-Kimball-like Hamiltonians [59], i.e., an admixture of spins and/or fermions, whose nonergodic dynamics has been recently investigated as a candidate for disorder-free localization [27–32].

To directly reveal this hidden structure, we introduce a nonlocal dual transformation, which maps Eq. (3) to three coupled transverse field Ising (TFI) chains [see Fig. 1(b) and Appendix B],

$$H^{\mathrm{KL}}_{\mathrm{dual}} = -\sum_i \left(j_m \mu^z_{g,i} + t_m \mu^x_{g,i}\mu^x_{g,i+1}\left(1+\mu^z_{r,i+1}\mu^z_{b,i+1}\right)\right) - \sum_i \left(j_e \mu^z_{b,i} + t_e \mu^x_{b,i}\mu^x_{b,i+1}\left(1+\mu^z_{g,i}\right)\right) - \sum_i \left(j_e \mu^z_{r,i} + t_e \mu^x_{r,i}\mu^x_{r,i+1}\left(1+\mu^z_{g,i}\right)\right), \quad (4)$$

where

$$\mu^x_{g,i} = \prod_{j\geqslant i} X_{r,j}X_{b,j+1}, \quad \mu^x_{r/b,i} = \prod_{j\geqslant i} Z_{g,j}Z_{r/b,j},$$

and $\mu^z_{g,i} = B_p(i)$, $\mu^z_{r/b,i} = A_s^{r/b}(i)$. This model features glassy dynamics for the $\mu_{g,r/b}$ degrees of freedom, associated to the anyonic excitations of the KL. For example, in the noninteracting limit $t_m = 0$ an effective description of $H^{\mathrm{KL}}_{\mathrm{dual}}$ reduces to two TFI chains coupled to the static $\mathbb{Z}_2$ gauge field, μ^z_g. These gauge degrees of freedom form a set of L constants of motion with trivial dynamics. Hence, an arbitrary initial nonzero density of fluxes ρ_m *energetically* suppresses charges' kinetic interactions [see Fig. 1(c)]. Indeed, a typical initial inhomogeneity of $\{\mu_g\} = \pm 1$ is dynamically manifested in a *self-generated disorder potential*,

$$t'_e(i) = t_e(1+\mu_{g,i}), \quad (5)$$

with the dilution distribution,

$$\mathcal{P}(t'_e) = (1-\rho_m)\delta(t'_e - 2t_e) + \rho_m \delta(t'_e), \quad (6)$$

where for a fixed value of ρ_m, different configurations of fluxes correspond to different realizations of disorder. In such a situation, dynamics of the whole system will be identical to that of two decoupled, disordered TFI chains in terms of $\hat{\mu}_{r/b}$, which are Anderson localized for any value of $\rho_m > 0$ [60]. An intriguing and simple picture of the topological aspect of such glassiness is that, during the propagation of e anyons across the system, they braid around the randomly filled plaquettes—characterized by the probability ρ_m—with a static $\mathbb{Z}_2$ gauge field μ_g. Thus, while passing each plaquette, e anyons experience a random phase dictated by semionic exchange angle, which leads to anyonic self-localization. This procedure is comparable with that presented in Ref. [32], in the sense that a nonergodic dynamics can be induced just through the presence of static gauge degrees of freedom.

III. ANYONIC SELF-LOCALIZATION AND QUASI MBL REGIME

The outlined glassy blueprint is inspiring to look for the counterpart of quasi MBL [30] in an Abelian many-body system. In analogy to the observed quasi MBL in a trivial admixture of heavy and light particles [27–31], one needs to choose the mass ratio of the quasiparticles to be large enough, as long as the "isolated bands" [29] due to finite-size effects is not manifested. In the KL, t_e (t_m) controls the strength of the effective disorder (interaction) as well as the effective mass of e (m) anyons [61]. Thus, we consider the limit $0 < t_m \ll t_e$, where m's have a large but finite effective mass. Now we initialize the whole system in a typical inhomogeneous configuration $|\psi_{N_m}\rangle$ of

$$N_m = \rho_m L$$

fluxes, which are selected near the middle of the spectrum of H^{KL}. Then, we compute the evolution of the flux inhomogeneity density under H^{KL},

$$\triangle\rho^2_m(t) \equiv \frac{1}{L}\sum_{p=1}^{L} \left|\langle\psi_{N_m}|(n^m_{p+1}(t) - n^m_p(t))|\psi_{N_m}\rangle\right|^2, \quad (7)$$

which vanishes for any perfect delocalized state. As illustrated in Figs. 2(a) and 2(b), for $t_m \gtrsim 0.01$ fast relaxation of the initial inhomogeneity due to resonance admixtures [27,28] takes place within the time scale $\tau_{\mathrm{int}} \sim t_m^{-1}$, while in the opposite limit, i.e., small t_m, the initial inhomogeneity plateau persists until τ_{int}. Moreover, the residual inhomogeneity remains even at later times $\tau_{\mathrm{eff}} \sim t_e/t_m^2$. Subsequent to this time, the collective slow dynamics eventually gives way to complete relaxation at τ_R. As discussed in Ref. [29], to ensure the robustness of the numerical results against finite-size effects, the density of states (DOS) must not display any isolated classical bands, which can be clearly seen in the insets of Fig. 2.

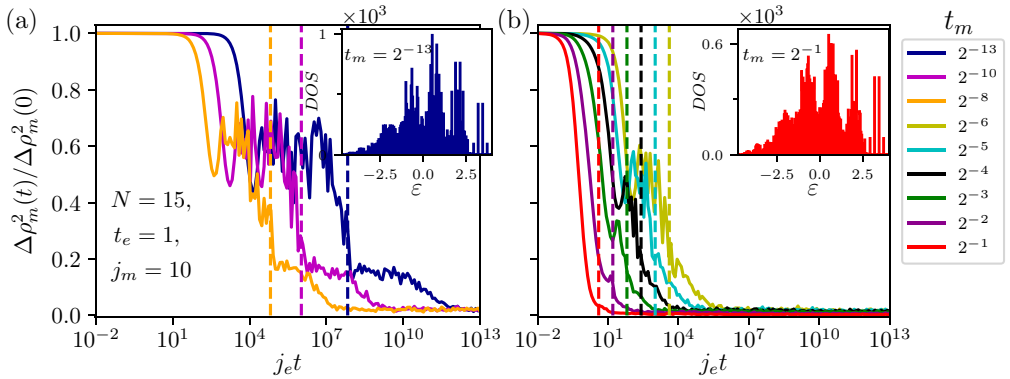

FIG. 2. Relaxation of the flux inhomogeneity density for $N = 15$ (spins) with fixed $t_e = 1$ and varying t_m, averaged over 150 random initial states $|\psi_{N_m}\rangle$, with $N_m = 3$ in the (a) fast and (b) slow dynamics regime. Vertical dashed lines represent time at τ_{eff}. (insets) DOS for the cases with largest and smallest mass ratio t_m/t_e.

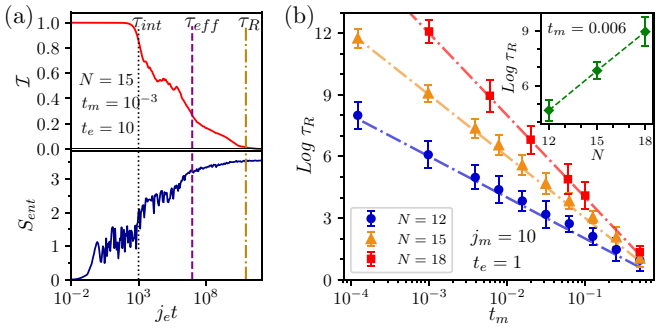

FIG. 3. (a) Upper panel: Relaxation of the time averaged inhomogeneity of fluxes for $N = 15$ and $t_e = 10$, in the quasi MBL regime at $t_m = 10^{-3}$, averaged over 150 initial states with $N_m = 3$. Lower panel: entanglement dynamics for a subsystem of size $N_A = 8$, averaged over 250 random product states. (b) The scaling behavior of τ_R versus t_m at fixed $t_e = 1$, for $N = 12,15,18$ with the initial total number of fluxes, $N_m = 2,3,4$, respectively. The dot-dashed lines denote the analytical estimation $\tau_R t_m \propto (t_e/t_m)^{N_m-1}$. (Inset) The expected exponentially diverging behavior of τ_R with system sizes at $t_m = 0.006$ in the quasi MBL regime.

To gain further insights on the nature of the three distinct time scales, $\tau_{\rm int} < \tau_{\rm eff} \leqslant \tau_R$, that characterize the relaxation dynamics of anyons, we have also looked at the growth of entanglement entropy $S_{\rm ent} = -\rho_A \ln \rho_A$ for half system A at strong disorder $t_e = 10$ [see Fig. 3(a)]. Prior to $\tau_{\rm int}$, charges perceive the fluxes as if they are immobile barriers. Hence, after an initial growth, $S_{\rm ent}$ saturates to the first plateau, conveying the single particle localization length of charges. Subsequent to $\tau_{\rm int}$ hybridization of fluxes arrives, which in turn intertwines with the charge dynamics. Thus, the entropy shows logarithmic growth until the finite-size dephasing of charges wins at the second plateau. At $\tau_{\rm eff}$, the dephasing of the fluxes sets in and the entanglement grows even more slowly to saturate eventually at τ_R. It is worth mentioning that the same time scales also determine the evolution of the quantity

$$\mathcal{I}(\tau) = \frac{\overline{\triangle\rho_m^2(\tau)} - \overline{\triangle\rho_m^2(\infty)}}{\overline{\triangle\rho_m^2(0)} - \overline{\triangle\rho_m^2(\infty)}}, \tag{8}$$

where

$$\overline{\triangle\rho_m^2(\tau)} \equiv \frac{1}{\tau}\int_0^\tau dt \triangle\rho_m^2(t), \tag{9}$$

[see Fig. 3(a)]. Moreover, the behavior of $\mathcal{I}(\tau)$ signifies that the full relaxation eventually occurs but at very late times. This anyonic slow dynamics is in contrast to true MBL in which an initial inhomogeneity never completely decays and resembles those characteristic behaviors observed in the previous proposal of quasi MBL [30].

Following the perturbative argument presented in Refs. [27,28], the finial decay time of the initial inhomogeneity in KL—due to collective off-resonance motion of N_m fluxes—should take place at time proportional to t_{CM}^{-1}, where t_{CM} is the effective hopping of the center of mass:

$$\tau_R \propto t_{CM}^{-1} \propto \frac{t_e^{N_m-1}}{t_m^{N_m}}, \tag{10}$$

which for a typical nonzero density of magnetic charges ($\rho_m \neq 0$) and in the thermodynamics limit scales exponentially with system size, i.e.,

$$\tau_R t_m \propto (t_e/t_m)^{\rho_m L}, \tag{11}$$

provided that the criteria for quasi MBL holds ($t_e \gg t_m$). To confirm this parametric dependence, in Fig. 2(b), we have plotted τ_R versus t_m at the fixed value of $t_e = 1$ for $N = 12,15$, and 18, which agrees with Eq. (10) very well.

For $N = 12,15$, we performed extensive exact diagonalization and averaged over 150 random initial configurations of magnetic charges with fixed total number of fluxes N_m. For $N = 18$, due to lack of special symmetries, e.g., $U(1)$, that can significantly decrease the effective Hilbert space dimension, we implemented another advanced method in order to reach system sizes far beyond exact diagonalization studies: (i) In the fast relaxation regime, i.e., $t_m \sim t_e$, we use a massively parallel time integration method [62–64] based on Chebyshev expansion that is suitable for simulating the dynamics up to the moderate times that are much larger than the typical value of τ_R in this regime. (ii) In order to compute τ_R for slow relaxation regime we simulate relaxation time trace via shift-and-invert Lanczos method [65]. To find a large portion of spectrum, we use the implementation of PETSc [62,63] and SLEPc [64] rely on MUMPS [66] to perform parallel sparse Cholesky factorization as a direct solver.

These numerical results illustrate a very good agreement with the rough estimation presented above in each set of data and imply the exponential dependence of τ_R on the system size with a growing number of fluxes in the quasi MBL regime [see inset of Fig. 2(b)]. This exponentially anyonic slow dynamics is comparable to the one which occurs in the presence of external disorder [57,58], but in contrast, here we deal with an arbitrary nonzero density of fluxes as well as generic perturbations in a translationally invariant system.

Lastly, we would like to address whether the fast relaxation in such anyonic liquids is followed by the viability of ETH in HES. In this respect, we discard the pair creation/annihilation of fluxes, which might happen as a result of $X_{r,i}X_{b,i+1}$ terms in Eq. (3). Typically, these recombination processes are less likely for the heavy particles in comparison with the light ones. Therefore, it is a reasonable assumption to consider,

$$\tilde{H}_{\rm KL} = \hat{P}_{N_m} H^{\rm KL} \hat{P}_{N_m}, \tag{12}$$

where $\hat{P}_{N_m}$ is the projection operator into the subspace with fixed N_m (see Appendix C). We evaluate $\mathcal{G} \equiv \langle n_p^m n_{p+1}^m \rangle$ as an ETH indicator in the simultaneous eigenstates of $\tilde{H}_{\rm KL}$ and momentum (hence we only consider $\mathcal{G}$ for $p = 1$) and collect the results from all momenta. Figure 4(a) quantifies $\mathcal{G}$ in different energy densities for $(t_e,t_m) = (1,0.001)$. In the whole energy intervals, the value of $\mathcal{G}$ is spread considerably in a wide range. On top of that, the distribution function $\mathcal{P}(\mathcal{G})$ near the middle of the band has a very broad half-width and peaks at different values as the system size is increased [right panel in Fig. 4(a)] indicating a strong nonergodic behavior. For the fast dynamics, e.g., $(t_e,t_m) = (1,0.5)$, the system rather obeys ETH prediction: DOS becomes continuous, $\mathcal{P}(\mathcal{G})$ sharply picked around its mean value and the width of the distribution decreases by increasing the system size, as illustrated in

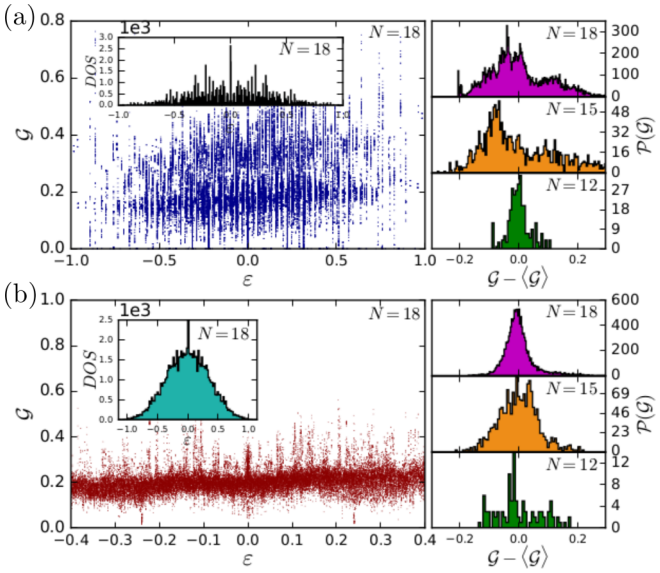

FIG. 4. (a) Failing of ETH for the case $(t_e,t_m) = (1,0.001)$. Left panel: The exception value of $\mathcal{G}$ in momentum eigenstates versus energy density. Inset displays DOS for $\tilde{H}_{\rm KL}$. Right panel: $\mathcal{P}(\mathcal{G})$ for all eigenstates in the energy window $\varepsilon \in [-0.09,0.09]$ in the middle of the energy band for different system sizes. The average value is removed from the distribution for visibility. (b) Manifestation of ETH for $(t_e,t_m) = (1,0.5)$. $\mathcal{P}(\mathcal{G})$ is plotted in the interval $\varepsilon \in (0,0.15]$. Results are reported for $(N,N_m) = (12,2)$, (15,3), and (18,3).

Fig. 4(b). Hence, whenever t_e and t_m are in the same order of magnitude, the fast relaxation occurs along with the validity of ETH in HES.

IV. RESILIENCE OF THE TOPOLOGICAL ORDER FOLLOWING A QUENCH

To further inspect the fingerprints of the emergent kinetic constraint in Eq. (4) on nonequilibrium anyonic dynamics, we proceed with the scenario of the quantum quench. We initially prepare the system in

$$|\phi_0\rangle = (1/2)(1 + \hat{W}_x)\big|\{n_p^m\},\{n_s^e\}\big\rangle, \tag{13}$$

where $\hat{W}_x$ is one of the two logical operators that encode the topological qubit, and $|\{n_p^m\},\{n_s^e\}\rangle$ is an exact eigenvector of $H_0^{\rm KL}$ [Eq. (1)] including a specific pattern of e's and m's. According to the SPT nature of $H_0^{\rm KL}$ (see Appendix. D), the corresponding eigenstates are short-range entangled and thus cold state. We are specially interested in those transitionally invariant pre-quench states with $\rho_m = 1$ and $\rho_e = 0$, wherein initial information is encoded in the subspace with maximum number of m anyons. By performing time integration based on Chebyshev expansion to evolve system under $H^{\rm KL}$, Eq. (3), we measure the spreading of the stored initial information as well as the nonequilibrium heating procedure over the course of time,

$$\Delta\mathcal{S} = \frac{S_{\rm ent}(t) - S_0}{S_{\rm page} - S_0}, \tag{14}$$

where $S_{\rm ent}(t)$, S_0, and $S_{\rm page}$ are bipartite entanglement entropies associated with $|\phi(t)\rangle$, $|\phi_0\rangle$, and an infinite temperature state [67], respectively. While for such a clean stabilizer code a fast thermalization is expected after the unitary time evolution from *ground state* [46], we show that away from this subspace thermalization is repressed for a finite range of parameters, even though the pre-quench state possesses a *regular* pattern of m and e anyons.

For the noninteracting limit $t_m = 0$, it follows from Eq. (5) that the dynamic of charges would be completely suppressed due to the presence of static fluxes in each plaquette. Indeed, turning on finite t_e within the full-flux sector could not modify eigenvalues and the corresponding eigenvectors relative to those in the pure KL. So, eigenstates within this sector do not mix with each other under the influence of Ising perturbations. Hence, regardless of the magnitude of j_m and t_e, the spreading of information is strictly impeded even in the absence of any explicit form of disorder in either the Hamiltonian or the initial state.

For $t_m \neq 0$, the flux occupation numbers are no longer constants of motion. Hence, to build up the tendency toward the survival of preparatory fluxes over the course of time, one needs to increase the value of flux mass gap, j_m [see Figs. 5(a) and 5(c)]. Consequently, the thermalization process slows down at a continually growing rate [see Figs. 5(b) and 5(c)]. Hence, scaling of the late time saturation value of $S_{\rm ent}$ with different subsystem sizes N_A reforms from volume law to area law, as depicted in Fig. 5(d). An approximate area law is observed for $j_m \gtrsim 4$, while for $j_m = 1, 2$ the scaling obeys volume law

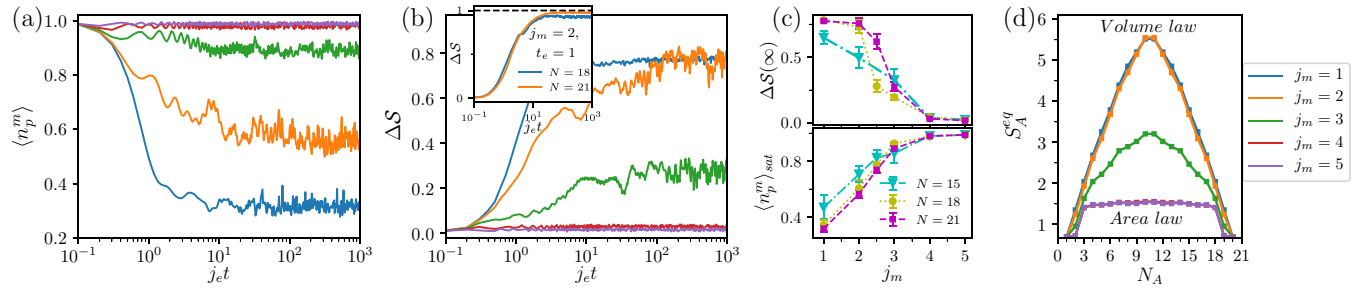

FIG. 5. (a) Evolution of the expectation value of $\hat{n}_p^m$ by varying the flux mass gap j_m, for $N = 21$, $t_e = 10$, $t_m = 0.6$ and the pre-quench state initialized in $\rho_m = 1$ and $\rho_e = 0$. Since both the Hamiltonian and initial state are translationally invariant, the results for all plaquettes are the same. (b) The information spreading, (c) late time saturation values, and (d) scaling of $S_{\rm ent}$ with different subsystem sizes N_A, at $j_e t = 10^3$, where $\langle n_p^m \rangle$ saturates to its long-time value. (Inset) The heating procedure in the ergodic phase, in which systems with sizes $N = 18$ and 21 could reach their thermal Gibbs state.

[68]. Notably, in the thermal regime, the system with sizes considered here [up to the Hilbert space dimension $\mathcal{D} \propto 10^6$] can reach its infinite temperature state [see inset of Fig. 5(b)], the behavior that is never observed in the systems suffering from finite-size effects.

V. DISCUSSIONS

We identified the anyonic self-localization as an emergent property purely rooted in the intrinsic statistics of the Abelian anyons and extended the so-called quasi MBL picture to self-correcting quantum codes. This provides a mechanism distinct by nature from the recent proposals on disorder-free localization [27,28,30,32,69]. Our results on anyonic self-induced disorder indicate that an exponentially glassy dynamics could be induced even (i) in *low-dimensional*, *clean*, and *simple-structure* models, and remarkably (ii) this glassiness is enhanced by *increasing* either the density of errors and/or environmental perturbations [28] (see also Appendix E). As already mentioned, this nonergodic dynamics could have a crucial consequence for the stability of topological quantum memories.

The scenario discussed in this paper could be generalized to 2D quantum double models such as the Levin-Wen model [70] or Kitaev's toric code. In these models, an anyon of type a can be transported from site i to site j along the directed path γ connecting the two sites through applying open string operators (Wilson line operators) of type a, W^a_γ. In order to mobilize anyons in the system and let them acquire kinetic energy, we can add $\sum_a \sum_\gamma g^a_\gamma W^a_\gamma$ to the ideal (exactly solvable) Hamiltonian, where g^a_γ is the amplitude of path γ. Now, imagine two distinct paths γ_1 and γ_2. The product of the two open string operators along γ_1 and $\overline{\gamma_2}$ (γ_2 with opposite direction), i.e., $W_c \equiv W^a_{\gamma_1} W^a_{\overline{\gamma_2}} = W^a_{\gamma_1}(W^a_{\gamma_2})^{-1}$, forms a closed string (Wilson loop operator). The resulting loop can take various quantized values depending on the total anyon charge inside path $\gamma_3 \equiv \gamma_1\overline{\gamma_2}$. Now suppose the resulting path, i.e., γ_3, encloses total anyon charge equal to b. The Wilson operator W_c measures the braid statistics between anyons a and b and is independent of path γ_3 (as far as it encompasses the anyon charge b). Therefore, $W^a_{\gamma_2} = W_c W^a_{\gamma_1}$. As a result, the total contribution of the two paths γ_1 and γ_2 is $(g^a_{\gamma_1} + g^a_{\gamma_2} W_c) W^a_{\gamma_1}$. Now, let us assume the two paths γ_1 and γ_2 are related via some symmetry operations, for instance the mirror symmetry with respect to the x axis. In that case, we must choose $|g^a_{\gamma_1}| = |g^a_{\gamma_2}|$ if we want to preserve that symmetry. Since W_c depends on the total anyon charge trapped inside loop γ_3 and it may take a different value upon the translation of γ_3, the perturbations can be viewed as disordered anyon hopping terms where the disorder is due to the nontrivial anyonic braiding statistics as discussed previously. Besides, as little progress has been made toward investigation of MBL in topologically ordered 2D systems, our study breaks ground for future research.

A closely related concept to quasi MBL in multicomponent systems is quantum disentangled liquid [69,71,72], wherein "post-measurement" of the anyon configuration is identical to the error syndrome; that is, the first step in the error-correcting protocol. It is tempting to see whether such a measurement procedure on a topological state supports this claim. Intuitively, could a quantum disentangled *spin* liquid be found there?

ACKNOWLEDGMENTS

We highly appreciate fruitful discussions and helpful comments by F. Alet, M. Najafi-Ivaki, M. Mohseni-Rajaee, and A. Pal. The authors would like to thank Sharif University of Technology for financial supports and CPU time from Cosmo cluster. A.V. was supported by the Gordon and Betty Moore Foundation's EPiQS Initiative through Grant No. GBMF4302.

APPENDIX A: KITAEV LADDER

We first briefly discuss the main properties of the KL Hamiltonian, H_0^{KL}, in (highly) excited states to give an insight on its nature as an anyonic liquid. In KL periodic-boundary condition in the leg direction leads to the global constraint $\prod_i A_s^{r/b}(i) = \mathbb{1}$, which ensures that (i) any energy level in the whole spectrum will have at least twofold degeneracy and (ii) $2L-1$ independent charge degrees of freedom are created/annihilated in pairs. However, fluxes can be created/annihilated singly in contrast to the 2D toric code on torus. One can also define the occupation operators of charges and fluxes as $\hat{n}^e_i = (1 - A_s^{r/b}(i))/2$ and $\hat{n}^m_i = (1 - B_p(i))/2$, respectively. In terms of occupation operators, H_0^{KL} simply counts the total number of e and m anyons in the system. The basis which diagonalizes H_0^{KL} has the following closed form in the occupation number representation:

$$\left|\{n^m_i\},\{r_i\}\right\rangle = \hat{P}_{\{n^m_i\}}\hat{g}_{\{r_i\}}|x+\rangle^{\otimes N}, \tag{A1}$$

where

$$\hat{P}_{\{n^m_i\}} = \prod_i \left(1 + (-1)^{n^m_i} B_p(i)\right)/2,$$
$$\hat{g}_{\{r_i\}} = \prod_{i\,\in\,\mathrm{D}} Z_i^{r_i}, \tag{A2}$$

and $|x+\rangle$ is the eigenstate of X, i.e., $X|x+\rangle = |x+\rangle$. $\hat{g}_{\{r_i\}}$ is a member of the Abelian group G (consisting of 2^{2L} different set of configurations, $r_i = \{0,1\}$), which performs all spin-flip operations for $2L$ spins placed on the global path D (see Fig. 6). By the action of G on the charge vacuum state, one can generate all 2^{2L-1} different independent charge configurations. $\hat{P}_{\{n^m_i\}}$ is the projection operator to the subspace with flux configuration, $\{n^m_i\}$, where a 2^L different set of $n^m_i = \{0,1\}$ can generate corresponding flux degrees of freedom. However, $\{r_i = 1;\ \forall i\}$ is a special case for which $W_z \equiv \hat{g}_{\{r_i=1\}}$ goes over the whole system on a homologically nontrivial path D. Accordingly, for any state $|\{n^m_i\},\{r_i\}\rangle$, there is a degenerate state,

$$\left|\{n^m_i\},\{\bar{r}_i\}\right\rangle = \hat{W}_z\left|\{n^m_i\},\{r_i\}\right\rangle,\ \ \hat{W}_z = \prod_{i\,\in\,D} Z_i, \tag{A3}$$

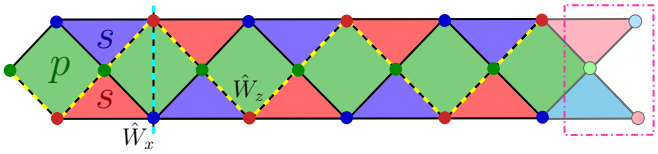

FIG. 6. KL as a surface code terminated in one direction. Dashed lines indicate topologically nontrivial path D and D'.

where $\hat{W}_z$ plays the role of *Wilson loop*, which creates a pair of charges on a vertex, rounds them across the system, and then annihilates them. This process is accompanied by changing topological sector of states (associated to different eigenstates of logical operator $\hat{W}_x = \prod_{i \in D'} X_i$) and can be interpreted as diffusion of unchecked errors across the ladder after a time proportional to the system size, a.k.a. logical error. Hence, generating glassy dynamics in highly-excited states (HES) of such disorder-free stabilizer codes impedes the mentioned procedure and puts forward a paradigm for realizing more stable quantum memories at finite temperature, the task which is assigned to the quasi many-body localization (quasi MBL) mechanism through this work.

As mentioned in the main text, the ground state of the KL model (with twofold degeneracy in the free charge and flux sectors $\{n_i^m = 0, r_i = 0;\ \forall i\}$) cannot be smoothly connected to a short range entangled state without breaking the Ising symmetries $\mathcal{P}_m$ and $\mathcal{P}_e$, defined in Eq. (2), explicitly or spontaneously. The action of these symmetries on occupation number basis Eq. (A1) can be interpreted as anyonic parity, such that $\mathcal{P}_m$ shows the *flux parity* and $\mathcal{P}_e$ represents the *charge parity* in the red or blue vertices.

APPENDIX B: BOUNDARY CONDITION FOR THE DUAL PSEUDOSPINS

In this section, we study the effect of the flux parity, defined in Eq. (2), on determining the boundary condition (BC) for pseudospins $\mu_{r/b}$. Because of the global constraint $\prod_i \mu^z_{r,i}\mu^z_{b,i} = \mathbb{1}$, $\mu_{r/b}$'s describe only $2L-1$ independent degrees of freedom. That being so, applying dual transformation on the original spins of the KL with periodic-BC results in a 1-to-2 mapping between $\mu_{r/b}$'s and original spins. One can consider two additional independent ancillary degrees of freedom, in the virtual $(L+1)$th unit cell of the ladder (see Fig. 6). According to our definition for blue and red pseudospins, $\mu^x_{r/b,i} = \prod_{j \geqslant i} Z_{g,j} Z_{r/b,j}$, the x component of ancillary pseudospins are product over an empty set, hence $\mu^x_{r,L+1} = \mu^x_{b,L+1} = 1$. On the other hand, the string operators $\mu^x_{r,1}$ and $\mu^x_{b,1}$ are two special cases that commute with H^{KL} and in terms of the original spins take the form $\mu^x_{r,1} = W_z$, $\mu^x_{b,1} = \mathcal{P}_m W_z$. Combination of these properties gives:

$$1 = \mu^x_{r,L+1} = \begin{cases} \mu^x_{r,1} & \text{if } \ W_z = +1 \\ -\mu^x_{r,1} & \text{if } \ W_z = -1. \end{cases} \tag{B1}$$

In fact, $\mu^x_{r,1}$ and $\mu^x_{b,1}$ are *dynamical variables* that are not independent from each other and determine the BCs on the μ's. So, according to Eq. (B1), the flux parity

$$\mathcal{P}_m = \mu^x_{r,1}\mu^x_{b,1} \equiv (-1)^{N_m} = \begin{cases} +1 \\ -1 \end{cases} \tag{B2}$$

determines the BC of the red and blue TFI chains in $H^{\mathrm{KL}}_{\mathrm{dual}}$ and relates them to each other in such a way that for the even parity two chains simultaneously have periodic BC or antiperiodic BC, but for the odd parity one chain has periodic BC while another must have antiperiodic BC and vice versa. In fact, the mentioned BCs, by doubling the size of the Hilbert space, establish a one-to-one mapping between all energy levels of $H^{\mathrm{KL}}_{\mathrm{dual}}$ and the perturbed KL Hamiltonian.

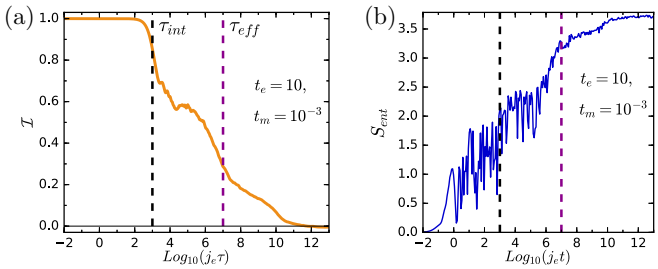

FIG. 7. (a) Relaxation of flux inhomogeneity and (b) growth of entanglement entropy for subsystem cut at eighth spin, corresponding to strong effective disorder governed by $\tilde{H}_{\mathrm{KL}}$ for $(N, N_m) = (15, 3)$, averaged over 200 random product states.

APPENDIX C: PROJECTED HAMILTONIAN

As mentioned in the main text, dynamics of the fluxes in our model is governed by the two-body ferromagnetic Ising interaction, $X_i X_j$ between the nearest neighbor spins, that sit on the legs of the ladder. Here, we would like to restrict our study to the effect of flux dynamics on localization or thermalization of finite energy states, therefore we discard the creation/annihilation of fluxes which might occur as a result of $X_i X_j$ terms. Typically, these recombination processes are less likely for the heavy particles in comparison with the light ones, equivalent to the condition $j_m \gg t_e > t_m$. Here, we impose this restriction by projecting the leg-Ising interaction onto the subspace with a fixed total number of flux by $\hat{P}_{N_m} = \sum'_{\{n_i^m\}} \hat{P}_{\{n_i^m\}}$, where $\hat{P}_{\{n_i^m\}}$ is defined in Eq. (A1), and the summation is restricted to those configurations in which $N_m = \sum_i n_i^m$ is fixed. In this respect, the projected Hamiltonian is given by $\tilde{H}_{\mathrm{KL}}$ defined in Eq. (12). The matrix elements of $\tilde{H}_{\mathrm{KL}}$ can only connect different configurations of the flux anyons with fixed N_m. Since the total number of fluxes, in addition to the flux parity, will be a constant of motion of $\tilde{H}_{\mathrm{KL}}$, using this projected Hamiltonian is more efficient for computational purposes. In this situation, the effective mass of heavy particles living in finite energy levels is inversely controlled by t_m in each fixed flux sector, j_m is an irrelevant parameter. To check the validity of this approach, in Fig. 7 we compute entanglement dynamics and relaxation of the initial inhomogeneity governed by $\tilde{H}_{\mathrm{KL}}$, which shows the same qualitative behavior in comparison to those governed by H^{KL} presented in the main text.

APPENDIX D: ROBUSTNESS OF SPT PHASE IN FINITE FLUX DENSITY

To reveal the effect of nonzero flux density on the robustness of SPT order, we consider $H^{\mathrm{KL}}_{\mathrm{dual}}$ with $t_m = 0$. First, in $\rho_m = 0$ the dual Hamiltonian reduces to two decoupled *clean* TFI chains. Accordingly, the system has a well-known phase transition at $t_e^c = j_e/2$. The paramagnetic phase for $t_e < j_e/2$ in the $\mu_{r/b}$ picture is identical to the $\mathbb{Z}_2 \times \mathbb{Z}_2$ SPT phase in the language of the original model [40], while $t_e > j_e/2$ is smoothly connected to the $j_e = 0$ fixed point and represents the trivial polarized phase. However, for $\rho_m > 0$ the TFI chains are no longer clean and effectively experience a random dilution disorder. According to the exact solution presented in Ref. [60],

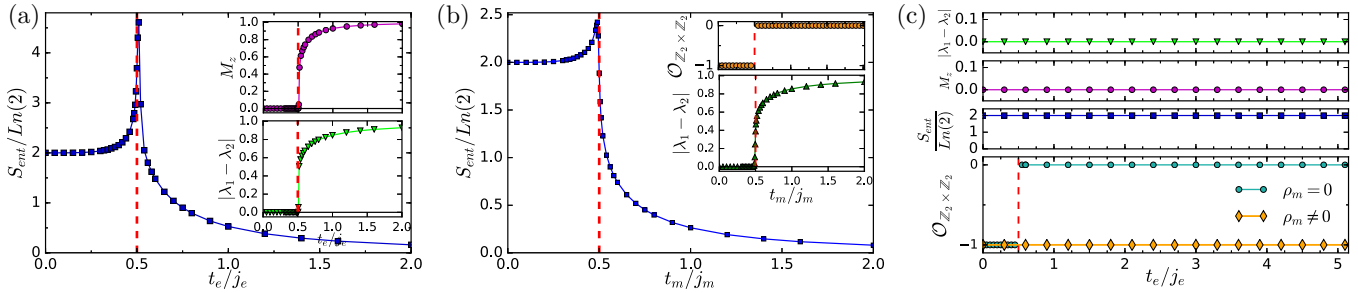

FIG. 8. (a) von-Neumann entropy S_{ent}, calculated by an implementation of iTEBD method with $\chi = 64$ for $H^{\text{KL}}(t_m = 0)$ in the $\rho_m = 0$ sector. The upper and bottom insets show magnetization M_z and the gap between two largest Schmidt coefficients $|\lambda_1 - \lambda_2|$, respectively. All data shows diverging behavior at $t_e^c = j_e/2$. (b) von-Neumann entropy computed for $H^{\text{KL}}(t_e = 0)$ in the $\rho_e = 0$ sector. The upper and bottom insets show $\mathcal{O}_{\mathbb{Z}_2\times\mathbb{Z}_2}$ defined in Eq. (D1) and the gap between two largest Schmidt coefficients, respectively. (c) The three top panels display the effect of nonzero density of fluxes on the same quantities plotted in (a). The lowest panel specifies the phase factor order parameter, $\mathcal{O}_{\mathbb{Z}_2\times\mathbb{Z}_2}$, which reveals robustness of the SPT order for $\rho_m \neq 0$.

for arbitrary (increasing) values of t_e, even an infinitesimal ρ_m spoils any long range magnetic order. For this reason, in the $\mu_{r/b}$-picture system is always in the paramagnetic phase, and thus the existence of m anyons favors the topological order.

Numerical approach.—We employed an infinite time-evolving block decimation (iTEBD) algorithm [73], which is based on an infinite matrix-product state (iMPS) representation to numerically check the validity of above analytical results. In the original model, for the case of $\rho_m = 0$, we compute the half-cut von-Neumann entanglement entropy, $S_{\text{ent}} = -tr(\rho_{L/2} \ln \rho_{L/2})$, where ρ is the ground state density matrix. The main plot of Fig. 8(a) shows a diverging behavior of S_{ent} at $t_e^c = j_e/2$. Moreover, the magnetization, $M_z = \sum_i Z_i/N$ [presented in the upper inset of Fig. 8(a)], shows a transition from a nonmagnetic phase for $t_e < j_e/2$ to a spontaneously symmetry breaking phase for $t_e > j_e/2$. The lower inset of Fig. 8(a) unveils the difference between the two largest magnitudes of Schmidt coefficients, $|\lambda_1 - \lambda_2|$, where the degeneracy of λ_1 and λ_2 for $t_e < j_e/2$ is the characteristic feature of SPT phase [74]. A similar behavior holds in the case $H^{\text{KL}}(t_e = 0)$ in the $\rho_e = 0$ sector, where the phase transition occurs at $t_m^c = j_m/2$ [see Fig. 8(b)]. Additionally, we compute the phase factor order parameter [75]:

$$\mathcal{O}_{\mathbb{Z}_2\times\mathbb{Z}_2} = \begin{cases} 0 & \text{if } |\eta_z| < 1 \text{ or } |\eta_x| < 1 \\ \frac{1}{\chi} tr(U_z U_x U_z^\dagger U_x^\dagger) & \text{if } |\eta_z| < 1 = |\eta_x| = 1, \end{cases} \tag{D1}$$

where η_z and η_x are the largest eigenvalues of the *generalized transfer matrix* [75] constructed by symmetry operators Σ^{IZZ} and Σ^{XXX}, respectively, and $U_z^\dagger$ and $U_x^\dagger$ are eigenvectors corresponding to them (here χ is the bond dimension of iMPS). The symmetry protected nontrivial phase, symmetry-breaking phase, and symmetry protected trivial phase are characterized by $\mathcal{O}_{\mathbb{Z}_2\times\mathbb{Z}_2} = \{-1, 0, 1\}$, respectively. The behavior of the mentioned quantities implies that for $t_e < j_e/2$ ($t_m < j_m/2$) the perturbed system at zero flux sector (zero charge sector) belongs to the $\mathbb{Z}_2 \times \mathbb{Z}_2$ quantum spin liquid phase.

Now, we consider the parent Hamiltonian $H_0^{'\text{KL}}$, which is different from H_0^{KL} in that we set $j_m \to j_m^{'} = -j_m$. The ground state of $H_0^{'\text{KL}}$ is in the full flux sector equivalent to the highest energy sector of H_0^{KL}. It can be shown that after adding the plaquette-Ising interaction (as charge kinetic term) to the $H_0^{'\text{KL}}$, the ground state of perturbed parent Hamiltonian, $H_{\text{KL}}^{'}$, remains in $\rho_m \neq 0$ sectors, provided that the rough estimate $t_e \lesssim j_m/2$ holds. It is worth mentioning that iTEBD algorithm does not guarantee the final wave function of $H_{\text{KL}}^{'}$ to remain in a sector with finite flux density for arbitrary enhancing value of t_e. Hence, mentioned constraint ensures that the zero-flux sector is not reachable as t_e is increased.

The results of our numerical simulation for $H_{\text{KL}}^{'}$ with $j_m^{'} = -10 j_e$ are presented in Fig. 8(c), which shows no evidence for a quantum phase transition at $\rho_m \neq 0$. The von-Neumann entropy is $2 \ln 2$, where magnetization is zero, the Schmidt coefficients are degenerate, and $\mathcal{O}_{\mathbb{Z}_2\times\mathbb{Z}_2} = -1$. All these results indicate the robustness of SPT order as a consequence of self-generated disorder. This effect is also comparable with Ref. [56], in which the *external* random field with dilution distribution stabilizes intrinsic topological order against *arbitrarily* strong magnetic fields.

APPENDIX E: THE ROLE OF INTERACTION AND EFFECTIVE TEMPERATURE

Here, we investigate the dependence of the nonergodic quench behavior on the interaction and effective temperature. Apart from the parameters j_m and t_m, the flux density in the pre-quench state and t_e can be seen as additional controlling parameters for initial energy density [through the relation $\varepsilon_{\rho_m} = -j_m(1 - \rho_m) - 2j_e$] and the strength of the effective disorder, respectively. By reducing the strength of interaction from $t_e = 10$ (see Fig. 5 in the main text) to $t_e = 1$, the information spreading escalates as shown in Fig. 9(a). Subsequently, as shown in Fig. 9(b), the scaling of entanglement changes behavior from area law to volume law, approximately around $j_m = 4.5$, which become greater than $j_m \sim 3$ for $t_e = 10$. Moreover, lowering the number of initial fluxes in the pre-quench state results in an upsurge in the heating process, in the way that the Ising perturbations adversely redesign the initial short-range state to a mixed one [see Fig. 9(c)]. As a result, increasing the effective temperature and strength of interaction ameliorates the resilience of topological order as well as robustness of the initial encoded information.

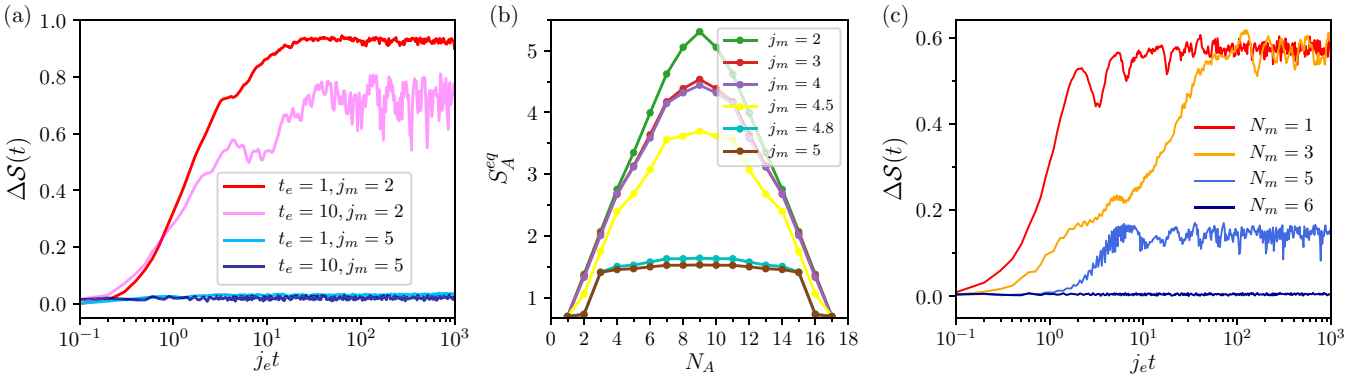

FIG. 9. (a) Spreading of the information for the pre-quench state initialized in $\rho_m = 1$, $t_m = 0.6$, and $N = 18$. (b) Scaling of S_{ent} with different subsystem sizes for $t_e = 1$, $t_m = 0.6$, and $\rho_m = 1$. (c) The effect of initial flux density on spreading of information for $t_e = 10$, $t_m = 0.3$, and $j_m = 5$.

[1] I. V. Gornyi, A. D. Mirlin, and D. G. Polyakov, Phys. Rev. Lett. **95**, 206603 (2005).
[2] D. Basko, I. Aleiner, and B. Altshuler, Ann. Phys. **321**, 1126 (2006).
[3] V. Oganesyan and D. A. Huse, Phys. Rev. B **75**, 155111 (2007).
[4] A. Pal and D. A. Huse, Phys. Rev. B **82**, 174411 (2010).
[5] B. Bauer and C. Nayak, J. Stat. Mech.: Theory Exp. (2013) P09005.
[6] J. Z. Imbrie, J. Stat. Phys. **163**, 998 (2016).
[7] P. W. Anderson, Phys. Rev. **109**, 1492 (1958).
[8] J. A. Kjäll, J. H. Bardarson, and F. Pollmann, Phys. Rev. Lett. **113**, 107204 (2014).
[9] M. Serbyn, Z. Papić, and D. A. Abanin, Phys. Rev. B **90**, 174302 (2014).
[10] M. Serbyn, M. Knap, S. Gopalakrishnan, Z. Papić, N. Y. Yao, C. R. Laumann, D. A. Abanin, M. D. Lukin, and E. A. Demler, Phys. Rev. Lett. **113**, 147204 (2014).
[11] M. Žnidarič, T. Prosen, and P. Prelovšek, Phys. Rev. B **77**, 064426 (2008).
[12] J. H. Bardarson, F. Pollmann, and J. E. Moore, Phys. Rev. Lett. **109**, 017202 (2012).
[13] R. Vosk and E. Altman, Phys. Rev. Lett. **110**, 067204 (2013).
[14] M. Serbyn, Z. Papić, and D. A. Abanin, Phys. Rev. Lett. **110**, 260601 (2013).
[15] J. M. Deutsch, Phys. Rev. A **43**, 2046 (1991).
[16] M. Srednicki, Phys. Rev. E **50**, 888 (1994).
[17] M. Rigol, V. Dunjko, and M. Olshanii, Nature (London) **452**, 854 (2008).
[18] D. A. Huse, R. Nandkishore, V. Oganesyan, A. Pal, and S. L. Sondhi, Phys. Rev. B **88**, 014206 (2013).
[19] A. Chandran, V. Khemani, C. R. Laumann, and S. L. Sondhi, Phys. Rev. B **89**, 144201 (2014).
[20] Y. Bahri, R. Vosk, E. Altman, and A. Vishwanath, Nat. Commun. **6**, 7341 (2015).
[21] A. C. Potter and A. Vishwanath, arXiv:1506.00592.
[22] N. Y. Yao, C. R. Laumann, and A. Vishwanath, arXiv:1508.06995.
[23] G. Carleo, F. Becca, M. Schiró, and M. Fabrizio, Sci. Rep. **2**, 243 (2011).
[24] W. De Roeck and F. Huveneers, Commun. Math. Phys. **332**, 1017 (2014).
[25] W. De Roeck and F. Huveneers, Phys. Rev. B **90**, 165137 (2014).
[26] J. M. Hickey, S. Genway, and J. P. Garrahan, J. Stat. Mech.: Theory Exp. (2016) 054047.
[27] M. Schiulaz and M. Müller, AIP Conf. Proc. **1610**, 11 (2014).
[28] M. Schiulaz, A. Silva, and M. Müller, Phys. Rev. B **91**, 184202 (2015).
[29] Z. Papić, E. M. Stoudenmire, and D. A. Abanin, Ann. Phys. **362**, 714 (2015).
[30] N. Y. Yao, C. R. Laumann, J. I. Cirac, M. D. Lukin, and J. E. Moore, Phys. Rev. Lett. **117**, 240601 (2016).
[31] L. Barbiero, C. Menotti, A. Recati, and L. Santos, Phys. Rev. B **92**, 180406 (2015).
[32] A. Smith, J. Knolle, D. L. Kovrizhin, and R. Moessner, Phys. Rev. Lett. **118**, 266601 (2017).
[33] M. Serbyn, Z. Papić, and D. A. Abanin, Phys. Rev. Lett. **111**, 127201 (2013).
[34] D. A. Huse, R. Nandkishore, and V. Oganesyan, Phys. Rev. B **90**, 174202 (2014).
[35] A. Chandran, I. H. Kim, G. Vidal, and D. A. Abanin, Phys. Rev. B **91**, 085425 (2015).
[36] V. Ros, M. Müller, and A. Scardicchio, Nucl. Phys. B **891**, 420 (2015).
[37] E. Dennis, A. Kitaev, A. Landahl, and J. Preskill, J. Math. Phys. **43**, 4452 (2002).
[38] A. Kitaev, Ann. Phys. **303**, 2 (2003).
[39] V. Karimipour, Phys. Rev. B **79**, 214435 (2009).
[40] A. Langari, A. Mohammad-Aghaei, and R. Haghshenas, Phys. Rev. B **91**, 024415 (2015).
[41] C. Castelnovo and C. Chamon, Phys. Rev. B **76**, 184442 (2007).
[42] C. Castelnovo and C. Chamon, Phys. Rev. B **77**, 054433 (2008).
[43] B. J. Brown, D. Loss, J. K. Pachos, C. N. Self, and J. R. Wootton, Rev. Mod. Phys. **88**, 045005 (2016).
[44] Z. Nussinov and G. Ortiz, Phys. Rev. B **77**, 064302 (2008).
[45] M. B. Hastings, Phys. Rev. Lett. **107**, 210501 (2011).
[46] Y. Zeng, A. Hamma, and H. Fan, Phys. Rev. B **94**, 125104 (2016).

[47] A. Kay, Phys. Rev. Lett. **102**, 070503 (2009).
[48] C. Chamon, Phys. Rev. Lett. **94**, 040402 (2005).
[49] I. H. Kim and J. Haah, Phys. Rev. Lett. **116**, 027202 (2016).
[50] R. Alicki, M. Horodecki, P. Horodecki, and R. Horodecki, Open Syst. Inf. Dyn. **17**, 1 (2010).
[51] D. Mazáč and A. Hamma, Ann. Phys. **327**, 2096 (2012).
[52] B. J. Brown, A. Al-Shimary, and J. K. Pachos, Phys. Rev. Lett. **112**, 120503 (2014).
[53] A. Hamma, C. Castelnovo, and C. Chamon, Phys. Rev. B **79**, 245122 (2009).
[54] F. L. Pedrocchi, A. Hutter, J. R. Wootton, and D. Loss, Phys. Rev. A **88**, 062313 (2013).
[55] O. Landon-Cardinal, B. Yoshida, D. Poulin, and J. Preskill, Phys. Rev. A **91**, 032303 (2015).
[56] D. I. Tsomokos, T. J. Osborne, and C. Castelnovo, Phys. Rev. B **83**, 075124 (2011).
[57] J. R. Wootton and J. K. Pachos, Phys. Rev. Lett. **107**, 030503 (2011).
[58] C. Stark, L. Pollet, A. Imamoğlu, and R. Renner, Phys. Rev. Lett. **107**, 030504 (2011).
[59] L. M. Falicov and J. C. Kimball, Phys. Rev. Lett. **22**, 997 (1969).
[60] R. B. Stinchcombe, J. Phys. C: Solid State Phys. **14**, L263 (1981).
[61] Generally, in a stabilizer Hamiltonian, one deals with two concepts of mass, i.e., effective mass and mass gap. The latter is defined as energy needed for creation/annihilation of anyons and controlled by j_e and j_m parameters.
[62] S. Balay, S. Abhyankar, M. Adams, P. Brune, K. Buschelman, L. Dalcin, W. Gropp, B. Smith, D. Karpeyev, D. Kaushik *et al.*, *Petsc users manual revision 3.7*, Tech. Rep. (Argonne National Lab. (ANL), Argonne, IL (US), 2016).
[63] S. Balay, W. D. Gropp, L. C. McInnes, and B. F. Smith, in *Modern Software Tools in Scientific Computing*, edited by E. Arge, A. M. Bruaset, and H. P. Langtangen (Birkhäuser Press, Boston, 1997), pp. 163–202.
[64] V. Hernandez, J. E. Roman, and V. Vidal, ACM Trans. Math. Softw. **31**, 351 (2005).
[65] To check the accuracy of extracted τ_R from this method we progressively increase the number of targeted eigenstates from 100 to 5500, which indicates the convergence of τ_R to its rough estimation given in the main text. We also considered different targeted energy densities, centered at $j_e/2$ and $j_e/4$, which does not show any qualitative difference. The reported results are averaged over 600 realizations of initial states and extracted data from targeted energy densities centered at $j_e/2$ and $j_e/4$.
[66] P. R. Amestoy, A. Guermouche, J.-Y. L'Excellent, and S. Pralet, Parallel Computing **32**, 136 (2006).
[67] D. N. Page, Phys. Rev. Lett. **71**, 1291 (1993).
[68] In this setting, we investigate the translationally invariant pre-quench states and the observed nonergodic behavior takes place even at the moderate value of t_m.
[69] T. Grover and M. P. A. Fisher, J. Stat. Mech.: Theory Exp. (2014) P10010.
[70] M. A. Levin and X.-G. Wen, Phys. Rev. B **71**, 045110 (2005).
[71] J. R. Garrison, R. V. Mishmash, and M. P. A. Fisher, Phys. Rev. B **95**, 054204 (2017).
[72] T. Veness, F. H. L. Essler, and M. P. A. Fisher, Phys. Rev. B **96**, 195153 (2017).
[73] R. Orús and G. Vidal, Phys. Rev. B **78**, 155117 (2008).
[74] F. Pollmann, A. M. Turner, E. Berg, and M. Oshikawa, Phys. Rev. B **81**, 064439 (2010).
[75] F. Pollmann and A. M. Turner, Phys. Rev. B **86**, 125441 (2012).